An internet server for pre-main sequence tracks of low- and intermediate-mass stars

L. Siess, E. Dufour, and M. Forestini

Observatoire de Grenoble, Laboratoire d'Astrophysique, Université Joseph Fourier, B.P. 53, 38041 Grenoble Cedex 9, France

Abstract. We present new grids of pre-main sequence (PMS) tracks for stars in the mass range 0.1 to 7.0 $M_\odot$. The computations were performed for four different metallicities (Z=0.01, 0.02, 0.03 and 0.04). A fifth table has been computed for the solar composition (Z=0.02), including a moderate overshooting. We describe the update in the physics of the Grenoble stellar evolution code which concerns mostly changes in the equation of state (EOS) adopting the formalism proposed by Pols et al. (1995) and in the treatment of the boundary condition. Comparisons of our models with other grids demonstrate the validity of this EOS in the domain of very low-mass stars. Finally, we present a new server dedicated to PMS stellar evolution which allows the determination of stellar parameters from observational data, the calculation of isochrones, the retrieval of evolutionary files and the possibility to generate graphic outputs.

Key words: equation of state – stars: evolution – stars: Hertzsprung–Russel (HR) and C-M diagrams – stars: pre-main sequence – astronomical data bases: miscellaneous

1. Introduction

Interest in modeling of very low-mass stars (VLMS) has grown steadily over the past decade, due to a large amount of work, both theoretical and observational. Brown dwarfs and very low-mass stars are now frequently discovered and the abundant literature in this domain attests to the vitality of this field. From these observations, we now realize that very low-mass stars represent a large fraction of the stellar population. However, the precise determination of the initial mass function, and more generally of stellar parameters and evolutionary states is still limited by the accuracy of stellar models. It is therefore desirable that different tracks be available in order to understand the theoretical discrepancies and also to estimate the uncertainties associated with the derivation of stellar parameters.

On the theoretical side, the computation of the structure of very low-mass stars is very challenging since it involves the micro-physics associated with dense, cold and partially degenerate matter. In the interior of VLMS, collective effects due to

Send offprint requests to: Lionel Siess

large densities become important and an accurate treatment of pressure ionization and Coulomb interactions is required. Also, in the cool atmosphere of VLMS, several molecules form and produce strong absorption bands that considerably modify the emergent spectrum. As a consequence, the stellar surface cannot be considered as a black body and stellar atmosphere models must also be used.

Since our last grids (Siess et al. 1997, hereafter SFD97), substantial improvements have been made in the Grenoble stellar evolution code that led us to the production of new grids of PMS tracks. The main modification to the code concerns the equation of state (EOS) which treats more accurately the behavior of cold and degenerate matter. In particular, we now take into account the effects associated with the pressure ionization and treat more carefully degeneracy conditions in stellar interior. We also updated the opacity tables using the latest release of the OPAL group and modified our surface boundary conditions using analytic fits to stellar atmosphere models. The updates to the code are described in Sect. 2 followed by a brief description of the grids. Then in Sect. 4 we compare our models to grids recently published by other groups. Finally, we describe a new server dedicated to PMS evolution.

2. The stellar evolution code

A general description of the stellar evolution code has already been presented in several papers (i.e. Forestini 1994, SFD97) and only subsequent modifications are discussed. They include updates in the opacity tables, in the treatments of the atmosphere and the incorporation of a new formalism for the equation of state.

2.1. Opacity tables

At high temperature (i.e. above 8000 K), we use the OPAL radiative opacities by Iglesias and Rogers (1996) which now include additional metal elements. The tables are interpolated in temperature, density and H, He, C, O and metal mass fraction using the subroutine provided by the OPAL group. However, for the computation of very low-mass stars ($M \lesssim 0.2\,M_\odot$), we had to extrapolate the opacity tables to $\log R = \log(\rho/T_6^3) = 4.0$ but this is of little effect since the internal region concerned

with this extrapolation ($T \gtrsim 10^5$ K) has an almost adiabatic behavior. Consequently, the temperature gradient is governed by the thermodynamics coming from the equation of state and is nearly independent of the opacity coefficient. Conductive opacities are computed from a modified version of the Iben (1975) fits to the Hubbard and Lampe (1969) tables for non-relativistic electrons, from Itoh et al. (1983) and Mitake et al. (1984) for relativistic electrons and from formulae of Itoh et al. (1984) as well as Raikh and Yakovlov (1982) for solid plasmas. Below 8000 K, we use the atomic and molecular opacities provided by Alexander and Fergusson (1994) as in SFD97.

2.2. Treatment of the atmosphere

The stellar structure is integrated from the center to a very low optical depth ($\tau = 0.005$) in the atmosphere. In the regions where $\tau < 10$, we constrain the atmospheric temperature profile (as well as the radiative pressure and gradient) to correspond to those coming from realistic atmosphere models determined by the integration of the radiative transfer equation. More specifically, we have performed one analytic fit of $T(\tau)$, as a function of effective temperature T_{eff}, surface gravity g_{eff} and metallicity Z which agrees with the atmosphere models to within 20% or less. The parameters of this fit are constrained by various atmosphere models, namely (1) Plez (1992) for $2500 < T_{\text{eff}} < 4000$ K, (2) Eriksson (1994, private communication, using a physics similar to Bell et al. 1976) up to 5500 K and (3) Kurucz's models (1991) computed with the ATLAS 12 code above 5500 K. Unfortunately, the lack of atmosphere models in some regions of the $Z - g_{\text{eff}}$ plane did not allow us to precisely determine the behavior of this fit at high gravity and/or non solar metallicities. This can potentially affect the modeling of very low-mass stars but considering the weak dependence of our fit on Z and g_{eff} compared to the one on T_{eff}, we decided to use this unique fit in all our computations instead of using a grey atmosphere approximation. This fit also provides a faster convergence in the surface layers due to the smooth profile of $T(\tau)$ and of its derivatives. Finally, let us mention that we define the effective temperature as $T_{\text{eff}} = (L/4\pi\sigma R^2)^{1/4}$ where L and R are estimated at $\tau = 2/3$.

2.3. Equation of state

In order to improve the description of the micro-physics relevant to VLMS, we have revisited the computation of the equation of state (EOS), adopting the scheme developed by Pols et al. (1995, hereafter PTEH). This new formalism is characterized by three main points:

- we adopt the chemical point of view (i.e. Saumon et al. 1995) where bound configurations (ions, molecules) are populated according to matter-photons and matter-matter interactions,
- we use the assumption of local thermodynamic equilibrium which allows the use of the Saha equations to determine the ion abundances as a function of the local values of temperature, T and number of electrons per unit mass, N_e,

- the plasma is described by three components, photons, ions and electrons, coupled only through the photo-ionization and photo-dissociation processes. Each component of the plasma is represented by an independent term in the Helmoltz free energy (Fontaine et al. 1977). Non-ideal corrections due to Coulomb shielding and pressure ionization are treated separately in an additional term whose expression has been fitted to the MHD EOS (Mihalas et al. 1988). This fit allows us to treat the regime of strong coupling while keeping the formalism of a separate additive term in the free energy to describe non-ideal effects (as explained in Saumon et al. 2000).

This new equation of state allows us to better take into account the effects of pressure ionization, partially degenerate matter and Coulomb interactions and provides very smooth profiles of the thermodynamic quantities since analytical expressions of all their derivatives can be obtained. Note that, as we will see in the next section, the computation of this EOS naturally introduces a new independent variable related to degeneracy.

2.3.1. A new variable

The general philosophy of this new EOS is to replace the density ρ (or pressure P) by a new independent variable which describes the electron degeneracy. To do so, we use the electron degeneracy parameter $\eta_e = \beta\xi_e$ where $\beta = 1/kT$ and ξ_e is the electron chemical potential. In this context, the density is given by

$$\rho = \frac{n_e(\eta_e, T)}{N_e(\eta_e, T, y_X)}, \tag{1}$$

where n_e, N_e and y_X are the number of electrons per unit volume, per unit mass and the molar fraction of a chemical element X, respectively.

N_e depends on η_e and T through the generalized Saha equations, and through the mass and charge conservation equations

$$N_e = \sum_{X,i} i N_{X^{i+}} \tag{2}$$

$$N_{X^{(i+1)+}} = N_{X^{i+}} \frac{\mathcal{Z}_{X^{(i+1)+}}}{\mathcal{Z}_{X^{i+}}} e^{-\eta_e - \Delta\eta_e - \beta\chi^{i+}} \tag{3}$$

$$N_{H_2} = \mathcal{Z}_{H_2} \left(\frac{N_H}{\mathcal{Z}_H}\right)^2 \quad \text{for } H_2 \tag{4}$$

$$y_X \mathcal{N}_a = \sum_i N_{X^{i+}} \quad \text{for } X \neq H \tag{5}$$

$$y_H \mathcal{N}_a = N_H + N_{H^+} + 2N_{H_2} + N_{H^-} \quad \text{for } H \tag{6}$$

where $N_{X^{i+}}$ represents the number per unit mass of the i times ionized atom X^{i+} (i can be negative for H^- for example), χ^{i+} its ionization potential, $\mathcal{Z}_{X^{i+}}$ its partition function and A_X its atomic molar mass. $\Delta\eta_e$ contains the contributions owing to the non-ideal effects of Coulomb interactions and pressure ionization which will be described in the following section. The use of η_e instead of ρ as the input variable for the Saha equations,

allows us to analytically derive the ionization states for all the desired elements anywhere in the star.

The number of electrons per unit volume n_e is then obtained in terms of η_e and T through the Fermi-Dirac integral

$$n_e = \frac{8\pi}{\lambda_c^3} \int_0^\infty \frac{y^2 dy}{e^{\frac{x}{T^*} - \eta_e} + 1} \qquad (7)$$

where $y = \frac{p}{m_e c} = x^2 + 2x$, λ_c is the electron Compton wavelength and $T^* = kT/m_e c^2$. This is a general definition which allows for relativistic electrons. In order to speed up the computation of n_e, we use polynomial fits to this integral. These fits have a simple form when expressed in terms of two variables, called f and g by Eggleton et al. (1973), arising from the asymptotic expansion of Eq. 7. Following these authors,

$$\eta_e = \ln(f) + 2 \times (\sqrt{1+f} - \ln(1 + \sqrt{1+f})). \qquad (8)$$

As a consequence, the variable $\ln(f)$ (hereafter $\ln f$), very well suited to describe the degeneracy of the plasma, is our new independent variable replacing ρ in the stellar structure equations. The change of variable $\rho(\ln f, T, y_i)$ is defined by Eqs. 1, 2, 7 and 8. In weakly degenerate conditions, $\ln f$ can be identified with a good approximation to the degeneracy parameter η_e while at high degeneracy f scales as η_e.

2.3.2. Physical ingredients of the EOS

The plasma is always considered as *partially* ionized for H, He, C, N, O and Ne. The other species are considered to be either neutral or totally ionized. Our tests indicate that for $M < 3\,M_\odot$, the structure and evolution of the stars are almost indistinguishable in both prescriptions (as far as PMS is concerned). In the more massive stars ($M \gtrsim 3\,M_\odot$) we report that models assuming total ionization for the heavy elements have initially a slightly shallower convective region but when the star reaches the ZAMS, these differences vanish.

Non-ideal effects include Coulomb shielding for all species and pressure ionization for H, He, C, N and O, except for H^-. Both effects have been incorporated following PTEH by means of analytic fits to the non-ideal terms in the Helmoltz free energy. The fit to the pressure ionization has been derived from the MHD EOS for a mixture $X=0.70$ and $Z=0.02$. Nevertheless, they have been used in all our computations, regardless of the chemical composition. According to Pols (private communication), this is a reasonable approximation since these fits give the expected behavior of pressure ionization as a function of T and of the degeneracy parameters (η_e or $\ln f$).

The computation of H_2 and H^- abundance is taken into account. For H_2, the partition function of Irwin (1987) is used in Eq. 3 below 16000 K and had to be extrapolated at higher temperatures to ensure the convergence of the model. This is certainly of little importance since in this region H_2 is insignificant. It must be noted that for very low-mass stars ($M \lesssim 0.4\,M_\odot$), H_2 becomes very abundant in the surface layers and must be included in the computations to ensure consistency between the atmosphere models (which include this molecule) and the EOS.
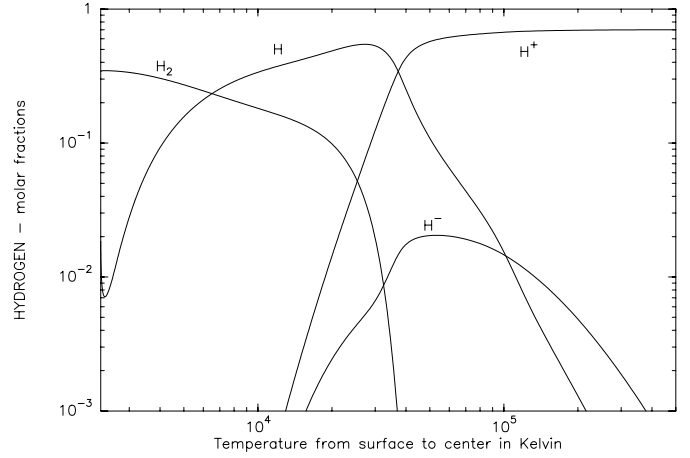
Fig. 1. Profiles of H, H^+, H^- and H_2 inside a $0.1\,M_\odot$ on the ZAMS. The star has an age of 8.36×10^9 yr, a solar composition and is located in the HRD at $T_{\rm eff} = 2776$ K and $L = 8.2 \times 10^{-4} L_\odot$

For example, in a $0.1\,M_\odot$ 50% of the hydrogen is trapped into H_2 at a temperature of 11800 K (Fig. 1). Further inside the star, this molecule cannot survive.

Due to its negative charge, the abundance of H^- derived from Eq. 3 is proportional to $\exp(\eta_e)$ instead of $\exp(-\eta_e)$. This different dependence of H^- abundance on the degeneracy parameter is not reproduced by the fit to the pressure ionization, thus preventing for the moment the treatment of this effect on this ion. This different behavior also explains why the peak of H^- is located at the maximum of the degeneracy parameter, around $T = 5 \times 10^4$ K where $\eta_e = 3.02$. We also verified that because of its small abundance in the encountered conditions, H^- has a negligible effect on the evolution tracks, even if its influence on the opacity coefficient can be large. Finally, in the central region of the star, H only subsists in its ionization state H^+.

Compared to Pols et al. (1995), our EOS presents slight modifications which mostly concern the treatment of ionization. More specifically, now that we compute the ionization states of C, N, O and Ne everywhere in the star, the elements for which ionization is not followed can be considered either completely ionized or neutral. The most recent partition function of Irwin (1987) is used for H_2 instead of Vardya's (1960) and the presence of H^- has been accounted for in the Saha equations. Apart from these modifications, the basic scheme and physical inputs (mainly the treatments of the non-ideal corrections and degeneracy) are the same. We checked that by adopting the same ionization treatment as PTEH (i.e. without the computation of H^- and assuming complete ionization for all the elements heavier than He), all the physical quantities derived form our EOS are comparable to that computed by PTEH to within less than 1%. Consequently, we refer the reader to these authors for a detailed comparison of this EOS with others. In particular, they found that due to the use of a simplified treatment of pressure ionization, this EOS can differ by up to 10% with the MHD and OPAL EOS, and even a bit more in the region of the $\rho - T$ plane delimited by the $3.0 < \log T < 4.5$ and $0 < \log \rho < 2$.

## 3. Pre-Main sequence computations

3.1. Initial models

Our initial models are polytropic stars that have already converged once with the code. The central temperature of all our initial models is below 10^6 K so deuterium burning has not yet taken place. The stars are completely convective except for $M \geq 6\,M_\odot$ where a radiative core is already present. For solar metallicity ($Z = 0.02$), we use the Grevesse and Noels (1993) metal distribution. For different Z, we scale the abundances of the heavy elements in such a way that their relative abundances are the same as in the solar mixture.

3.2. The grids

Our extended grids of models includes 29 mass tracks spanning the mass range 0.1 to $7.0\,M_\odot$. Five grids were computed for four different metallicities encompassing most of the observed galactic clusters ($Z = 0.01, 0.02, 0.03$ and 0.04) and, for the solar composition ($Z = 0.02$), we also computed a grid with overshooting, characterized by $d = 0.2H_p$, where d represents the distance (in units of the pressure scale height H_p measured at the boundary of the convective region) over which the convective region is artificially extended. An illustration of these grids is presented in Fig. 2. Our computations are standard in the sense that they include neither rotation nor accretion. The Schwarzschild criterion for convection is used to delimit the convective boundaries and we assume instantaneous mixing inside each convective zone at each iteration during the convergence process.

During the PMS phase, the completely convective star contracts along its Hayashi track until it develops a radiative core and finally, at central temperatures of the order of 10^7 K, H burning ignites in its center. The destruction of light elements such as ^{2}H, ^{7}Li and ^{9}Be also occurs during this evolutionary phase. Deuterium is the first element to be destroyed at temperatures of the order of 10^6 K. The nuclear energy release through the reaction ^{2}H(p,γ)^{3}He temporarily slows down the contraction of the star. Then, ^{7}Li is burnt at $\sim 3 \times 10^6$ K shortly followed by ^{9}Be. For a solar mixture, our models indicate that stars with mass $\leq 0.4\,M_\odot$ remain completely convective throughout their evolution. We also report that in the absence of mixing mechanisms, stars with $M > 1.1\,M_\odot$ never burn more than 30% of their initial ^{7}Li.

The account of a moderate overshooting characterized by $d = 0.20H_p$, significantly increases the duration of the main sequence (MS) for stars possessing a convective core and provides additional Li depletion during the PMS phase. More quantitatively, the MS lifetime of a $1.2\,M_\odot$ star is increased by 25%, this percentage then decreases to level off at around a 15% increase for $M \gtrsim 3\,M_\odot$. Surface depletion of Li occurs only in stars with $0.4 < M \lesssim 1.3$ for which the temperature at the base of the convective envelope can reach 3×10^6 K. Our models including overshooting indicates that Li is much more efficiently depleted around $0.8\,M_\odot$, where its abundance is $\sim 3 \times 10^5$ smaller than in a standard evolution.
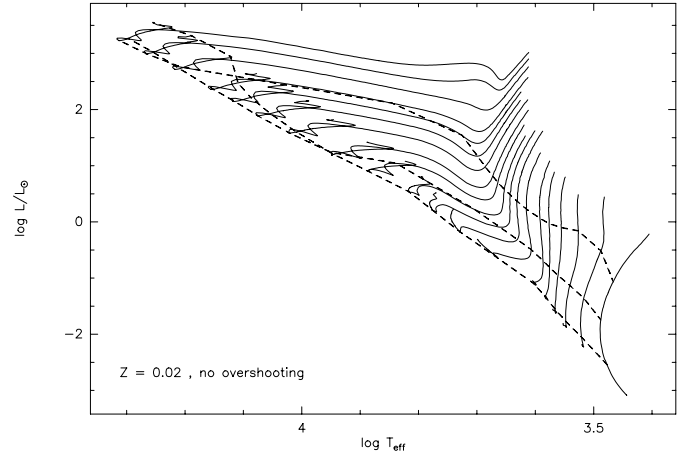
Fig. 2. Evolutionary tracks from 7.0 to $0.1\,M_\odot$ for a solar metallicity (Z=0.02 and Y=0.28). Isochrones corresponding to 10^6, 10^7 and 10^8 (dashed lines) are also represented. This figure has been generated using our internet server

3.3. Our fitted solar model

With the above physics, we have fitted the solar radius, luminosity and effective temperature to better than 0.1% with the MLT parameter $\alpha = 1.605$ and an initial composition $Y = 0.279$ and $Z/X = 0.0249$ that is compatible with observations. The values used for this fit are quite similar to those obtained by other modern stellar evolution codes (see e.g. Brun et al. 1998). Our sun, computed in the standard way, i.e. without the inclusion of any diffusion processes, has the following internal features

  – at the center: $T_c = 1.552 \times 10^7$ K, $\rho_c = 145.7\,\mathrm{g\,cm^{-3}}$, $Y_c = 0.6187$ and the degeneracy parameter $\eta_c = -1.527$;
  – at the base of the convective envelope: $M_\mathrm{base} = 0.981999\,M_\odot$, $R_\mathrm{base} = 0.73322\,R_\odot$, $T_\mathrm{base} = 1.999 \times 10^6$ K and $\rho_\mathrm{base} = 1.39610^{-2}\,\mathrm{g\,cm^{-3}}$.

These numbers are in very close agreement with other recently published standard models (see e.g. Brun et al. 1998, Morel et al. 1999, Bahcall & Pinsonneault 1996).

In our grid computed with overshooting, we found that the 1 $M_\odot$ model maintains a small convective core of $\sim 0.05\,M_\odot$ during the central H burning phase. This would consequently be the case for the fitted sun but present day helioseismic observations cannot exclude this possibility (e.g. Provost et al. 2000).

4. Comparison with other studies

In this section we compare our PMS tracks with the computations made available by the groups listed in Table 1. These comparisons show the accuracy of the EOS and the pertinence of our models in the domain of VLMS.

Pre-main sequence tracks differ from one group to another due to differences in the constitutive physics (EOS, convection), but also in the treatment of the surface boundary conditions. In the last decade, a tremendous amount of work has been done to

Table 1. PMS stellar models used in the comparisons

X	Z	Group	Code
0.725	0.019	Baraffe et al. (1998)	BCAH
0.680	0.020	Charbonnel et al. (1999)	Geneva
0.691	0.019	D'Antona & Mazzitelli (1997)	DM97
0.699	0.019	Swenson et al. (1994)	SW94
0.703	0.020	Siess et al. (1997)	SFD97
0.703	0.020	This study	

better understand the physical processes taking place in the extreme regime of high density and low temperature encountered in the interior of VLMS. Three main EOS have emerged: the MHD EOS used by the Geneva group and by DM97, the SCVH EOS (Saumon et al. 1995, hereafter SCVH95) used by Baraffe et al. (1998, hereafter BCAH) and the OPAL EOS (Rogers et al. 1996) used by DM97 in the regime of high temperature. Comparisons between these different EOS (SCVH95, Rogers et al. 1996, Chabrier & Baraffe 1997, Charbonnel et al. 1999) showed a good agreement within their domain of validity. For example, the MHD and SCVH EOS gives very similar results in the mass range $0.4 \lesssim M \lesssim 0.8\,M_\odot$.

Fig. 3 shows that, the morphology of our tracks is very similar to the BCAH and Geneva models, for all the considered masses. This is strong evidence that we correctly follow the thermodynamics involved in these objects. This is not surprising since, as mentioned in Sect. 2.3.2, we treat the non-ideal effects through analytical fits to the MHD EOS. In comparison, our previous tracks (long dashed-dotted lines) were systematically too red and their paths were very different from the new ones. This is due in part to the fact that H_2 was not accounted for in the computations and also because the treatment of the non-ideal effects was less accurate. As a consequence, the internal structure of our old models was less centrally condensed and the stellar radius slightly larger compared to our new models.

At the lower mass end (M=0.10 and $0.20\,M_\odot$), the similarity with BCAH models is striking, as effective temperature differences are $\lesssim 50\,K$ (much less than observational uncertainties along the Hayashi tracks!). In particular, this shows that our boundary conditions (Sect. 2.2) are in reasonably good agreement with the much more sophisticated atmosphere models used by BCAH. We see, however, that in the domain of very low mass stars ($M \lesssim 0.4\,M_\odot$) strong morphological differences are present. More specifically, we observe (Fig. 3) that the DM97 and SW94 tracks present a strong inflexion in their Hayashi path which is not reproduced by the other groups. Several reasons can be put forward to explain these differences. First DM97 uses a convection model which differs substantially from the commonly used standard MLT prescription. As shown by D'Antona and Mazzitelli (1998), this can result in $T_{\rm eff}$ differences as large as $\sim 200\,K$ along the Hayashi line (see also below). Secondly, in this mass range the morphology of the evolutionary tracks is particularly sensitive to the EOS and to the different treatments of the thermodynamics. Finally, their use of a grey atmosphere approximation is certainly not satisfactory for modeling cool
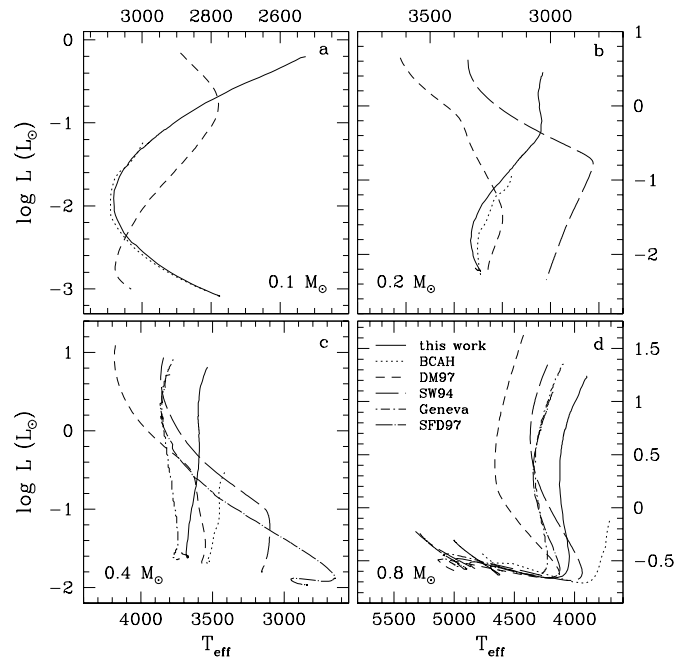
Fig. 3. HR diagrams comparing the different PMS tracks for the models listed in Table 1

stars whose emergent spectrum diverges significantly from a black body. In order to estimate the impact of using a grey atmosphere treatment in our stellar evolution code, we have also computed some additional tracks for different masses. We report that the non-grey atmosphere models are systematically cooler than the grey ones, as a result of molecular blanketing in the outermost layers (e.g. Chabrier et al. 1996). This probably also explains why the Geneva models, which use the same treatment of convection with a similar value for MLT parameter ($\alpha = 1.6 \pm 0.1$), are systematically hotter than ours.

For higher mass stars ($M \gtrsim 0.6\,M_\odot$), the morphology of the tracks becomes quite similar, as the non-ideal physical effects and the molecular absorption in the atmosphere vanish. The shifts in $T_{\rm eff}$ between the different tracks mainly result from the different chemical compositions and/or values of α in the MLT and can be as large as $200\,K$. In particular, the Hayashi tracks of the BCAH models become increasingly cooler as the stellar mass increases compared to all the other tracks. This most probably results from their smaller value of the MLT parameter ($\alpha = 1$), the effect of which is only significant above $\sim 0.6M_\odot$ (Chabrier and Baraffe 1997) and is to shift the tracks towards lower $T_{\rm eff}$. The fact that species heavier than H and He are not accounted for in the BCAH EOS could be part of the explanation as well. Finally, for the most massive stars ($M > 1.0\,M_\odot$), the morphology of the tracks is very similar. We notice however that our models are slightly cooler than the DM97 tracks by $\sim 100\,K$.

A comparison of the isochrones shows that our tracks are generally slightly more luminous than those of others. Consequently, for a given luminosity, the stellar age estimated from our models will be smaller, the relative effects being more pro-

nounced for younger stars. The discrepancy between the different isochrones is particularly strong below 10^6 yr, where an age determination remains, in any case, very misleading. This is, in part, due to the fact that early in the evolution, the results still depend on the initial state of the star (Tout et al. 2000).

Aside from the above-mentioned explanations for the discrepancies between the tracks, other physical ingredients, usually not reported in the literature, may also affect the evolutionary path of a PMS stars. Consequently, the origin of some of the observed discrepancies cannot be clearly identified. To illustrate this, we will now demonstrate that, even within the MLT, different prescriptions to solve the third polymonial equation for the convective gradient give rise to different degrees of superadiabadicity and thus a different location of the star in the HRD. Indeed, the $T_{\rm eff}$ location of a fully convective PMS stars is very sensitive to the degree of superadiabadicity in the sub-photospheric layers which in turn depends on the prescription used to compute the convective temperature gradient (see e.g. D'Antona & Mazzitelli 1998). We performed a series of tests using two different formalisms for the computation of the convective gradient, namely the Cox (1984, Chap. 14) and the Kippenhahn and Weigert (1991, Chap. 7) formalisms. The latter, used in our grids, leads in the superadiabatic region to a temperature gradient $\sim 20\%$ higher than that derived from the Cox formalism. This translates into effective temperature shifts of the Hayashi tracks of 100 to 300 K, depending on the stellar mass. The Cox solutions have systematically smaller radii and the Hayashi lines are consequently bluer. Finally, with the receding of the convective envelope, the degree of superadiabadicity decreases and the temperature shift reduces to ~ 100 K. These differences mainly result from the assumed "form factor" used in the MLT formalism. Indeed, the shape of the convective cells directly affects the radiative loss efficiency and a change in the form factor can be compensated by a modification to the α parameter. We refer the reader to Henyey et al. (1965) for a detailed discussion of the arbitrariness of some constants used in the MLT. Among other numerical tests, the evolution of the structure of PMS stars does not depend at all on the prescription used to write the gravothermal energy production rate ε_{grav} (i.e. using the internal energy, the entropy or the pressure; see Kippenhahn & Weigert 1991, Chap. 4). This is due to our completely consistent treatment of the thermodynamics with our EOS formalism.

Given the relatively good agreement between the different EOS involved in this comparison, the physical and numerical treatment of convection is certainly the most influent parameter for the modeling of fully convective PMS. It can account for $T_{\rm eff}$ differences as large as 300 K. Faced with our poor knowledge of convection, large discrepancies between the different sets of tracks are unfortunately inevitable.

5. Internet interface to stellar model requests

The internet site located at http://www-laog.obs.ujf-grenoble.fr/activites/starevol/evol.html offers several services to take advantage of our stellar model database. Among these facilities, it is possible to compute an isochrone, to determine the stellar parameters of a star knowing its position in the HR diagram, to draw a specific HR diagram and of course, and to retrieve all the evolutionary files.

For the computation of isochrones, the user specifies the metallicity, and ages and selects the mass tracks entering the computation of the isochrone. The results are displayed on the screen and can be saved in a file. We also give the luminosity, effective temperature, and radius as well as the colors and magnitudes corresponding to the location of a given star at any specified age. We use the conversion table provided by Kenyon and Hartmann (1995) and display the different colors in the Cousin system. It is also possible to ask for further information and get, for example, the surface Li abundance, the central temperature or the extent of the convective envelope for the set of stars selected to compute the isochrones.

The other facility is the determination of stellar parameters. The user specifies the coordinates of a star in the HR diagram using either the luminosity or magnitude and $T_{\rm eff}$ or colors and then, the program computes the theoretical track that passes through this observational point. This procedure allows the determination of the stellar age, mass and radius assuming the star is on its pre-main sequence track. If requested, additional information such as surface chemical composition, central properties or moments of inertia can also be provided.

The third facility deals with graphic outputs. In this page, the user can plot HR diagrams in any combination of color and magnitude. It is also possible to zoom in by stating limits, to superpose isochrones and/or the ZAMS.

6. Conclusion

We presented new pre-main sequence evolutionary tracks for low- and intermediate-mass stars. Comparisons of our models with other PMS tracks indicate rather strong discrepancies in the regime of very low-mass stars ($M \lesssim 0.5\,{\rm M_\odot}$). Our tracks are very similar, in morphology and effective temperature, to those computed by Baraffe et al. (1998) and the Geneva group (Charbonnel et al., 1999). This similarity is a strong indicator that our treatment of the EOS and boundary conditions is correct. Conversely, we report strong deviations of these tracks with those of D'Antona and Mazzitelli (1997), especially below 0.3 M$_\odot$. For higher mass stars, the morphology of the tracks is similar and effective temperature differences $\lesssim 200$ K are noted, partly due to different mixing length parameter values and chemical compositions. Comparisons of the isochrones, indicates age determination remains, in any case, very uncertain below 10^6 yr. Finally, we present our internet server which provides several facilities to use and take advantage of our large database of PMS stellar models.

References

Alexander D.R., Ferguson J.W., 1994, ApJ 437, 879

Bahcall J.N., Pinsonneault M.H., 1996, AAS 189, 5601B

Baraffe I., Chabrier G., Allard F., Hauschildt P.H., 1998, A&A 337, 403, BCAH

Bell R.A., Eriksson K., Gustafsson B., Nordlund A., 1976, A&A 23, 37

Brun A.S., Turck-Chieze S., Morel P., 1998, ApJ 506, 913

Chabrier G., Baraffe I., 1997, A&A 327, 1039

Chabrier G., Baraffe I., Plez B., 1996, ApJ 459, L91

Charbonnel C., Däppen W., Schaerer D., Bernasconi P.A., Maeder A., et al., 1999, A&AS 135, 405

Cox J., 1984, "Principle of Stellar Structure", Gordon and Bridge, Science Publishers

D'Antona F., Mazzitelli I., 1994, ApJS 90, 467

D'Antona F., Mazzitelli I., 1997, in: Cool Stars in Clusters and Associations, eds R. Pallavicini and G. Micela, Mem. S. A. It., 68, 807, DM97

D'Antona F., Mazzitelli I., 1998, in: Brown Dwarfs and Extrasolar Planets, ASP Conference Series, eds. R. Rebolo, E. Martin, M.R. Zapatero Osorio, p. 442

Eggleton P.P., Faulkner J., Flannery B.P., 1973, A&A 23, 325

Eriksson K. 1994, private communication, see Sect. 2.2

Fontaine G., Graboske H.C., Van Horn H.M., 1977, ApJS 35, 293

Forestini M., 1994, A&A 285, 473

Grevesse N., Noels A., 1993, in: Origin and Evolution of the Elements, eds Prantzos N., Vangioni-Flam E., Cassé M.

Henyey L., Vardya M.S., Bodenheimer P., 1965, ApJ 142, 841

Hubbard W.B., Lampe M., 1969, ApJS 18, 297

Hummer D.G., Mihalas D., 1988, ApJ 331, 794

Iben I., 1975, ApJ 196, 525

Iglesias C.A., Rogers F.J., 1996, ApJ 464, 943

Irwin A.W., 1987, A&A 182, 348

Itoh N., Mitake S., Iyetomi H. Ichimaru S., 1983, ApJ 273, 774

Itoh N., Kohyama Y., Matsumoto N., Seki M., 1984, ApJ 285, 758

Kenyon S.J., Hartmann L. 1995, ApjS 101, 117

Kippenhahn R., Weigert A., 1991, Stellar Structure and Evolution, Springer-Verlag

Kurucz R.L., 1991, Stellar Atmospheres: Beyond Classical Models. eds. Crivallery L., Hibeny I., Hammer D.G., NATO ASI Series, Kluwer, Dordrecht

Mihalas D., Hummer D.G., Däppen W., 1988, ApJ 331, 815

Mitake S., Ichimaru S., Itoh N., 1984, ApJ 277, 375

Morel P., Pichon B., Provost J., Berthomieu G., 1999, A&A 350, 275

Plez B., 1992, A&AS 94, 527

Pols O.R., Tout C.T., Eggleton P.P., Han Z., 1995, MNRAS 274, 964, PTEH

Provost J., Berthomieu G., Morel P., 2000, A&A 353, 775

Raikh M.E., Yakovlev D.G., 1982, ApSS 87, 193

Rogers F.J., Swenson F.J., Iglesias C.A., 1996, ApJ 456, 902

Saumon D., Chabrier G., Van Horn H.M., 1995, ApJS 99, 713, SCVH95

Saumon D., Chabrier G., Wagner D.J., Xie X., 2000, in: High Pressure Research, Gordon and Breach publishers

Siess L., Forestini M., Dougados C., 1997, A&A 324, 556, SFD97

Swenson F.J., Faulkner J., Rogers F.J., Iglesias C.A., 1994, ApJ 425, 286, SW94

Tout C.A., Livio M., Bonnell I.A., 2000, MNRAS 310, 360

Vardya M.S., 1960, ApJS 4, 281